A Full-Wave Analysis of an Arbitrarily Shaped Dielectric Waveguide Using Green's Scalar Identity

J. Charles, H. Baudrand, and D. Bajon

Abstract—**An integral equation analysis is proposed to determine the phase constant of an arbitrarily shaped dielectric waveguide. The main feature of this approach is the use of Green's scalar identity in which only simple contour integrals have to be evaluated. Different scalar Green's functions are considered to satisfy the boundary conditions for the electric and magnetic fields in each region. This approach is combined with the boundary element technique with linear elements for the computation. The case of the rectangular dielectric image waveguide is first discussed, and numerical results are found to be consistent with other theories and experiments. Also, the cases of hollow rectangular and semicircular image waveguides are analyzed and numerical results are presented.**

I. Introduction

The principal reason for the renewed interest in dielectric image lines is that the metallic wall structures cause attenuation owing to the skin effect in the range from millimeter to optical waves. Thus dielectric guiding structures are more suitable for millimeter-wave integrated circuits than microstrip transmisson lines. A number of theoretical studies of dielectric image waveguides have been presented in recent years [1]–[10]. Most of those methods are currently based on effective dielectric constant approximations or use accurate mode-matching techniques for their analysis. Schlosser *et al.* [1], Marcatili [2], and Goell [3] were the first to use accurate mode-matching techniques. Miao *et al.* [10] proposed a simple effective dielectric constant approach to analyze dielectric waveguides and hollow rectangular image guides.

Kazuhiko [5] and Solbach *et al.* [6] presented a calculation of the field distribution and phase constant of rectangular dielectric image lines. More recently, domain integral equation methods have been proposed [13]–[15]. Pichot [13] gave an exact numerical solution based on vector integral equations to investigate the diffused channel waveguide. Kolk *et al.* [15] used a domain integral equation representation in which the kernel of the integral consists of a dyadic Green's function to study integrated optical channel and ridge waveguides in stratified media. Bagby *et al.* [14] presented a polarization electric field integral equation; a Herztian potential Green's dyadic was used as the kernel of the integral for studying a generalized integrated dielectric waveguiding system.

The main feature of our proposed method is the use of Green's scalar identity and scalar Green's functions in which the transverse components of the electric and magnetic fields are expressed in terms of their longitudinal components for the analysis of the general structure shown in Fig. 1. Unlike the integral methods given in [13]–[15], our formulation is developed so as to use only simple contour integrals in the equations. This theoretical approach is combined with the boundary element technique with linear elements for the computation. Similar numerical methods have been proposed [11], [12] for the analysis of waveguide discontinuities; also, boundary element techniques were developed by Brebbia in his two books [17], [18].

Manuscript received July 5, 1990; revised October 3, 1990.

The authors are with the Laboratoire de MicroOndes, Institut National Polytechnique, E.N.S.E.E.I.H.T., 2, rue Charles Camichel, 31071 Toulouse Cedex, France.

IEEE Log Number 9144286.

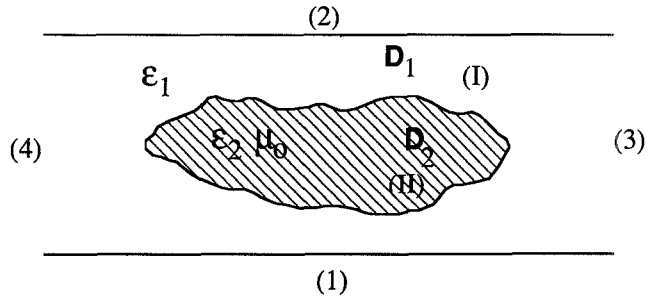

Fig. 1. Cross-sectional view of the waveguide to be analyzed: (*1*) and (*2*) are electric boundaries; (*3*) and (*4*) are magnetic or electric boundaries.

After subdividing the boundary (c) of the dielectric into segments, a linear variation of the electric and magnetic fields is assumed on each element. The equations are then combined to form a single matrix equation. Since the electric and magnetic fields do not satisfy the same boundary condition, two sets of scalar Green's functions are considered in each region of the structure. By imposing the condition that the determinant of the matrix be zero, the unknown phase constant is determined. Some infinite series present in the Green's functions have to be approximated for the numerical evaluation. Another advantage of this approach is that the shape of the waveguide may be arbitrary.

By this method various guiding structures have been studied and we have compared our results with other numerical techniques and with approximate solutions available in the literature. To illustrate the capability of this approach we also demonstrate the dispersion characteristics of a hollow semicircular dielectric image waveguide.

II. Formulation of the Problem

The general geometry of the analyzed structure is shown in Fig. 1. The subscript $i=1,2$ refers to regions I and II. The Green's functions corresponding to each region (I and II) are defined by G_i; these must satisfy the inhomogeneous Helmholtz equation:

$$\left(\nabla_s^2 + k_i^2 - \beta^2\right)G_i(r/r') = -\delta(r-r'), \qquad k_i^2 = \omega^2\mu_0\epsilon_i \quad (1)$$

where β is the unknown phase constant, and k_i is the wavenumber in the dielectric regions. The quantities ϵ_1 and ϵ_2 are the permittivities in regions I and II respectively and μ_0 is the permeability of free space. The boundary conditions in the domain D_1 are either the homogeneous Neumann conditions $\partial\Psi/\partial n = 0$ or the Dirichlet condition $\Psi = 0$. If $\partial\Psi/\partial n = 0$, then the potential Ψ is the longitudinal component H_z of the magnetic field. We then choose G_1 so that $\partial G_1/\partial n = 0$ on the limits of the domain D_1. If $\Psi = 0$, the potential Ψ is the longitudinal component E_z of the electric field: $G_1 = 0$ on the boundary of D_1.

The choice of the Green's function will not be the same for the electric and the magnetic field (see Appendix I). In region I the normal n is oriented from region I toward II. The scalar

0018-9480/91/0600-1029$01.00 ©1991 IEEE

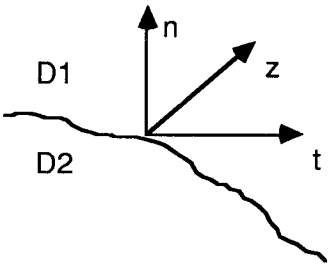

Fig. 2. Orientation of the direct coordinate system.

potential Ψ satisfies the propagation equation:

$$(\nabla_s^2 + k_i^2 - \beta^2)\Psi = 0$$

and from Green's formula we have

$$\Psi(r) = \int_c [G_i(r/r')(\partial_n \Psi)_i - \Psi(\partial_n G_i)(r/r')_i]\, dl.$$

The partial normal and tranverse derivatives are denoted by $\partial_n \cdot$ and $\partial_t \cdot$. The Green's functions corresponding to the electric and magnetic fields are denoted by G_e and G_h respectively. Then, in the domains I and II we can write

$$E_z = \hat{G}_{ei1}(\partial_n E_z)_i - \hat{G}_{ei2} E_z \quad \text{and} \quad H_z = \hat{G}_{hi1}(\partial_n H_z)_i - \hat{G}_{hi2} H_z.$$

In the above equations $\hat{G}_{e,hi1}$ and $G_{e,hi2}$ are the following operators:

$$\hat{G}_{e,hi1} \cdot = \int_1 G_{e,hi}(r/r') \cdot dl \quad \text{and} \quad G_{e,hi2} \cdot = \int_l \partial_n G_{e,hi}(r/r') \cdot dl.$$

The tangent to the boundary separating regions I and II is oriented so that the (n, t, z) coordinate system is direct (see Fig. 2). The divergence theorem shows that the signs of the integrals in domain I must change; the expressions for the longitudinal electric and magnetic fields are then given by

$$E_z = (-1)^i \left[\hat{G}_{ei1}(\partial_n E_z)_i - \widehat{G_{ei2}} E_z\right] \tag{2}$$

$$H_z = (-1)^i \left[\hat{G}_{hi1}(\partial_n H_z)_i - \widehat{G_{hi2}} H_z\right]. \tag{3}$$

From Maxwell's equations we can define the transverse components of the electric and magnetic fields E_T and H_T:

$$E_T = \frac{1}{k_i^2 - \beta^2}(-j\beta\partial_t E_z + j\omega\mu\partial_n H_z)$$

$$H_T = \frac{1}{k_i^2 - \beta^2}(-j\beta\partial_t H_z + j\omega\epsilon_i\partial_n E_z).$$

From the continuity of the electric and magnetic fields on the interface of the two regions, $E_{T1} = E_{T2}$ and $H_{T1} = H_{T2}$, the following expressions can be obtained:

$$a\partial_t E_z + b_1(\partial_n H_z)_1 + b_2(\partial_n H_z)_2 = 0 \tag{4}$$

$$a\partial_t H_z + c_1(\partial_n E_z)_1 + c_2(\partial_n E_z)_2 = 0 \tag{5}$$

where the coefficients a, b_1, b_2, c_1, and c_2 are given by

$$a = -j\beta\frac{(k_2^2 - k_1^2)}{(k_1^2 - \beta^2)(k_2^2 - \beta^2)} \qquad b_1 = j\omega\mu\frac{1}{k_1^2 - \beta^2}$$

$$b_2 = -j\omega\mu\frac{1}{k_2^2 - \beta^2}$$

$$c_1 = j\omega\epsilon_1\frac{1}{k_1^2 - \beta^2} \quad \text{and} \quad c_2 = j\omega\epsilon_2\frac{1}{k_2^2 - \beta^2}.$$

For transferring (2) and (3) from region I to region II we have to express $(\partial_n H_z)_1$ and $(\partial_n E_z)_1$ in terms of $(\partial_n H_z)_2$ and $(\partial_n E_z)_2$ by using (4) and (5):

$$(\partial_n H_z)_1 = -\frac{b_2}{b_1}(\partial_n H_z)_2 - \frac{a}{b_2}(\partial_t E_z) \tag{6}$$

$$(\partial_n E_z)_1 = -\frac{c_2}{c_1}(\partial_n E_z)_2 - \frac{a}{c_1}(\partial_t H_z). \tag{7}$$

Substituting (6) and (7) into expressions (2) and (3), we obtain the following matrix:

$$\begin{bmatrix} (1-\hat{G}_{e_{12}}) & -\frac{a}{c_1}\hat{G}_{e_{11}}\partial_t & -\frac{c_2}{c_1}\hat{G}_{e_{11}} & 0 \\ -\frac{a}{b_1}\hat{G}_{h_{11}}\partial_t & (1-\hat{G}_{h_{12}}) & 0 & -\frac{b_2}{b_1}\hat{G}_{h_{11}} \\ (1+\hat{G}_{e_{22}}) & 0 & -\hat{G}_{e_{21}} & 0 \\ 0 & (1+\hat{G}_{h_{22}}) & 0 & -\hat{G}_{h_{21}} \end{bmatrix} \cdot \begin{bmatrix} E_z \\ H_z \\ \partial_n E_z \\ \partial_n H_z \end{bmatrix} = \mathbf{0} \tag{8}$$

III. Green's Functions

The Green's functions of domain I are calculated to satisfy the boundary conditions for G_e and G_h. We give two expressions for these functions, which have been computed for the case of two finite ground planes with consideration given to electric and magnetic sidewalls (see Appendix I). In the case of infinite ground planes the corresponding Green's function is given by (9). In this expression the series converges very slowly:

$$G = j\Pi \sum_{n=-\infty}^{\infty} \left[H_0^{(2)}(k|r - r_n'|) + H_0^{(2)}(k|r - r_n''|)\right] \tag{9}$$

where

$$r_n' = a_x[2nh + x_0] + a_y y_0 \qquad r_n'' = a_x[2nh - x_0] + a_y y_0.$$

In the above relations h is the distance between the two ground planes, $k^2 = k_i^2 - \beta^2$, and $H_0^{(2)}$ is the zero-order Hankel function of the second kind. These series can be approximated by the following expressions when $kh \gg 1$:

$$\frac{2}{\sqrt{k^3 h\pi N}} \exp\left(-j\frac{3}{4}\pi\right) \exp\left(2jkh\sqrt{N} - jkx\right) \phi_1(x_0) \tag{10}$$

where $\phi_1(x_0) = \cos(kx_0)$ for G_h and $\phi_1(x_0) = \sin(kx_0)$ for G_e. In domain II the Green's function is given by

$$-\frac{j}{4}H_0^{(2)}(kr)$$

(see [11] and [17]).

IV. Numerical Implementation

Consider N_m points on the contour of the dielectric with coordinates denoted by x_m and y_m. In this case, the contour is divided into N_m subintervals, where the mth segment is defined by the coordinates x_m, y_m and x_{m+1}, y_{m+1}. It will be convenient

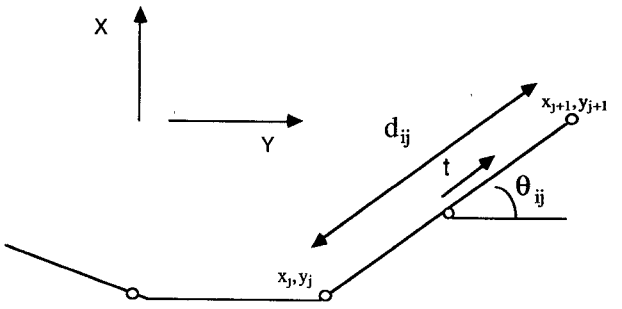

Fig. 3. The ith subinterval on the contour of the dielectric.

to make the following definition:

$$x_{Nm+1} = x_1 \quad \text{and} \quad y_{Nm+1} = y_1.$$

Also, we can describe the mth segment as a set of $x(t)$ and $y(t)$ functions defined by two parametric equations:

$$x(t) = x_m + t \sin\theta_m \tag{11a}$$

$$y(t) = y_m + t \cos\theta_m \tag{11b}$$

with $-d_m/2 \leqslant t \leqslant d_m/2$ (see Fig. 3).

Considering the above definitions, we suppose that the unknown functions $(E_z, H_z, \partial_n E_z, \partial_n H_z)$ vary linearly over the segment. These functions, denoted by Ψ, are then defined by the nodal points Ψ_m, Ψ_{m+1} and the interpolation functions by $\Phi_1 = 1/2(1-t)$ and $\Phi_2 = 1/2(1+t)$. So Ψ can be expressed in the following form:

$$\Psi(x,y) = [\Phi_1, \Phi_2] \begin{bmatrix} \Psi_m \\ \Psi_{m+1} \end{bmatrix}. \tag{12}$$

The final system to be computed is given in Appendix II.

V. Numerical Results

In this section we present some numerical results of various dielectric waveguides. This method was applied to analyze several structures with finite ground planes (Fig. 4) and infinite ground planes (Figs. 6 and 7). In the case of a structure having infinite ground planes, and when the values of hk are much greater than the wavelength (λ) (about $hk \sim 100\lambda$), the Green's function given by (9) can be approximated by expression (10). Therefore, very fast convergence of the series is obtained. For structures with finite ground planes, expressions (13) and (14) are used.

A Gaussian elimination technique is used for the evaluation of the determinant of the equation matrix given in Appendix II.

The calculation of our problem was performed on a HP personal computer. The dimension of the matrix equation is equal to $4n$, where n is the number of subintervals used to describe the contour of the dielectric. The dispersion characteristics corresponding to the three lowest order modes of the rectangular dielectric image line are shown in Fig. 4. Good accuracy in the results of the phase constant compared with those given by Solbach [6] and Marcatili [2] has been obtained. The convergence of our numerical results for the structure of Fig. 4 has been investigated by increasing the number of segments. The variation of the phase constant of the dominant mode with respect to the number of segments has been demonstrated in Fig. 5. From this figure it was found that by taking four segments, the error in the results was less than 1.8% compared with those reported in [6].

The hollow image guides (Fig. 6 and 7) have a number of interesting characteristics for millimeter-wave applications. For instance, the hollow core may be used to control the propagation constant without altering the exterior dimensions of these guides. It is well known that above a certain frequency there exists symmetric and antisymmetric modes. They can be regarded as two strongly coupled image guides.

The dispersion characteristics of the first dominant modes of the rectangular hollow image guide (Fig. 6) were computed. The discrepancy between our results and those presented by Itoh and Miao [10] is approximately less than 2%. The reasons for this difference have been explained in [10]. But our numerical results are found to be consistent with those presented in [16] using the transverse operator technique. We have also studied circular dielectric structures. The propagation constants of the dominant and first odd mode of a hollow semicircular dielectric image guide are plotted in Fig. 7. About 12 segments were used to compute the dispersion characteristics for this structure.

VI. Conclusion

A full-wave analysis using domain integral equations for the study of an arbitrarily shaped dielectric waveguide has been presented. The approach was combined with the boundary element technique with linear elements for the computation. We have demonstrated the capability and accuracy of our approach by comparing our numerical results with those available in the literature. We have noticed that even by taking a small number of segments for describing the contour of the dielectric, good accuracy in the results was obtained. Further, the convergence test for the numerical results obtained for a simple structure has been carried out. However, in order to reduce the computation time for the analysis of more complicated structures, series that converge more rapidly have been determined. In addition, this method can be used to analyze various structures. For example, shielded microstrip lines and field effect transistor structures are being analyzed by this approach after introducing two new equations for the conductors.

Appendix I

The Green's functions corresponding to the electric field, G_e, and magnetic field, G_h, are given in the following form (see [19]):

$$G_e(x_0 y_0 / xy) = \sum_{n=1}^{\infty} \frac{\gamma_n^e}{w} \varnothing_e(y) \begin{cases} \operatorname{sh}(\theta_n x) \operatorname{sh}(\theta_n (x_0 - b)), & x \leqslant x_0 \\ \operatorname{sh}(\theta_n (x - b)) \operatorname{sh}(\theta_n x_0), & x \geqslant x_0 \end{cases} \tag{13}$$

$$G_h(x_0 y_0 / xy) = \sum_{n=1}^{\infty} \frac{\gamma_n^h}{w} \varnothing_h(y) \begin{cases} \operatorname{ch}(\theta_n x) \operatorname{ch}(\theta_n (x_0 - b)), & x \leqslant x_0 \\ \operatorname{ch}(\theta_n (x - b)) \operatorname{ch}(\theta_n x_0), & x \geqslant x_0 \end{cases} \tag{14}$$

where

$$\theta_n = \frac{n\pi}{p} \alpha_n \quad \text{if } \left(\frac{p}{n\pi}\right)^2 (\beta^2 - k_i^2) > 1$$

$$\theta_n = i \frac{n\pi}{p} \alpha_n \quad \text{if } \left(\frac{p}{n\pi}\right)^2 (\beta^2 - k_i^2) < 1$$

$$\alpha_n = \sqrt{\left| 1 + \left(\frac{p}{n\pi}\right)^2 (k^2 - k_i^2)^2 \right|}; \quad \frac{\gamma_n^e}{w} = -\frac{2}{p} \frac{\cos\beta_n y_0}{\theta_n \operatorname{sh}\theta_n b}$$

$$\frac{\gamma_n^h}{w} = -\frac{2}{p} \frac{\sin\beta_n y_0}{\theta \operatorname{sh}\theta_n b} \quad \text{and} \quad \beta_n = \frac{n\pi}{p}.$$

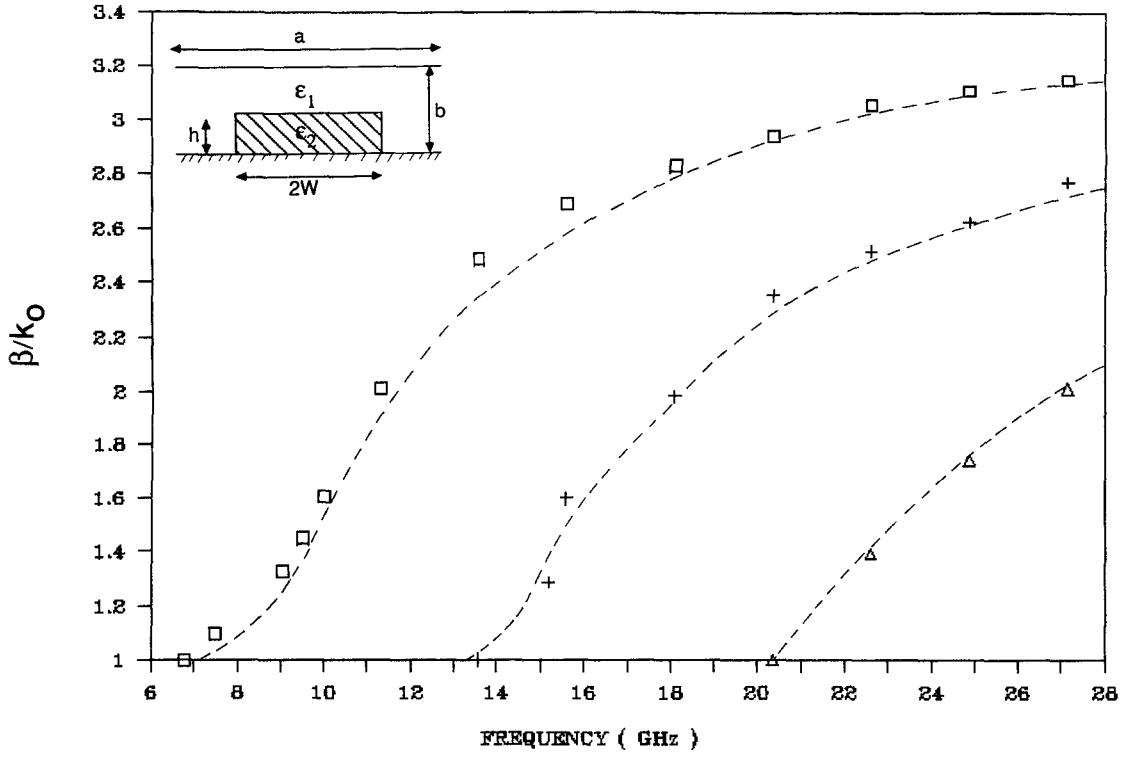

Fig. 4. Normalized phase constant of the rectangular dielectric image waveguide versus the frequency for $W/h = 1$, $a/b = 1$, $\epsilon_{r1} = 1$, and $\epsilon_{r2} = 12$. □ EH11 mode; + EH21 mode; Δ HE31 mode; ---- ref. [6]; □, +, Δ: our results.

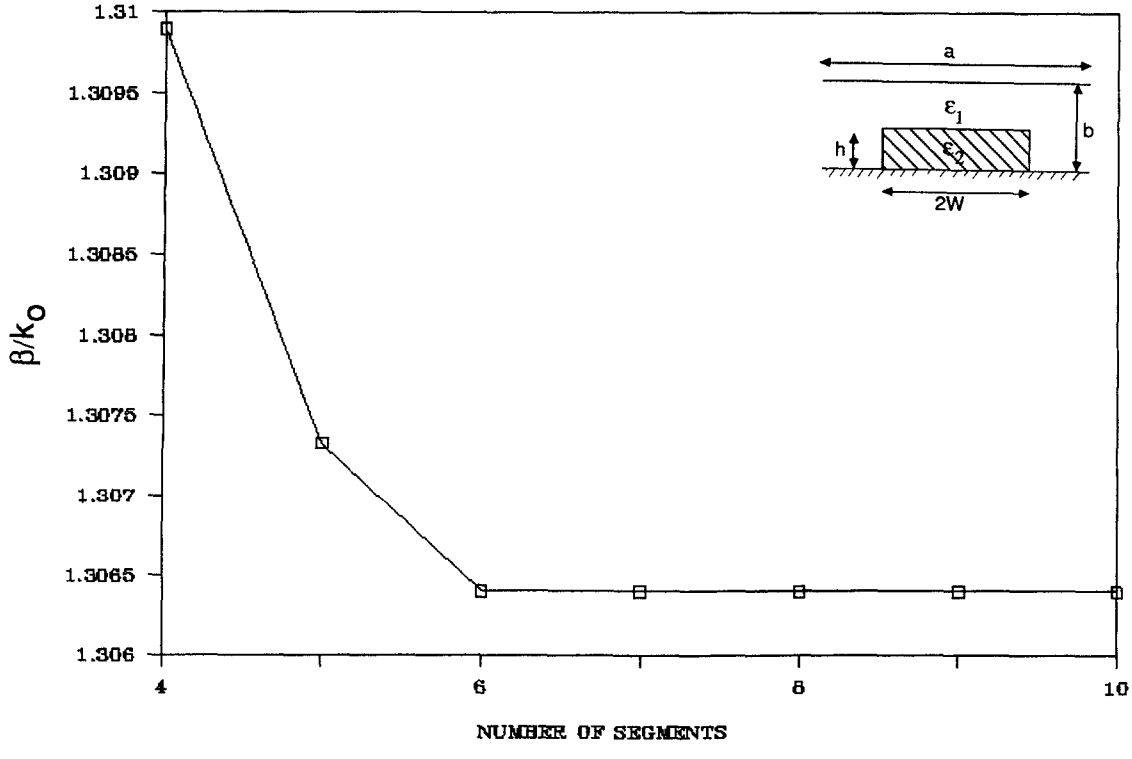

Fig. 5. Convergence test. Variation of the normalized phase constant versus the number of segments for $f = 47.5$ GHz, $w/h = 1$, $a/b = 1$, $\epsilon_{r1} = 1$, and $\epsilon_{r2} = 2.22$.

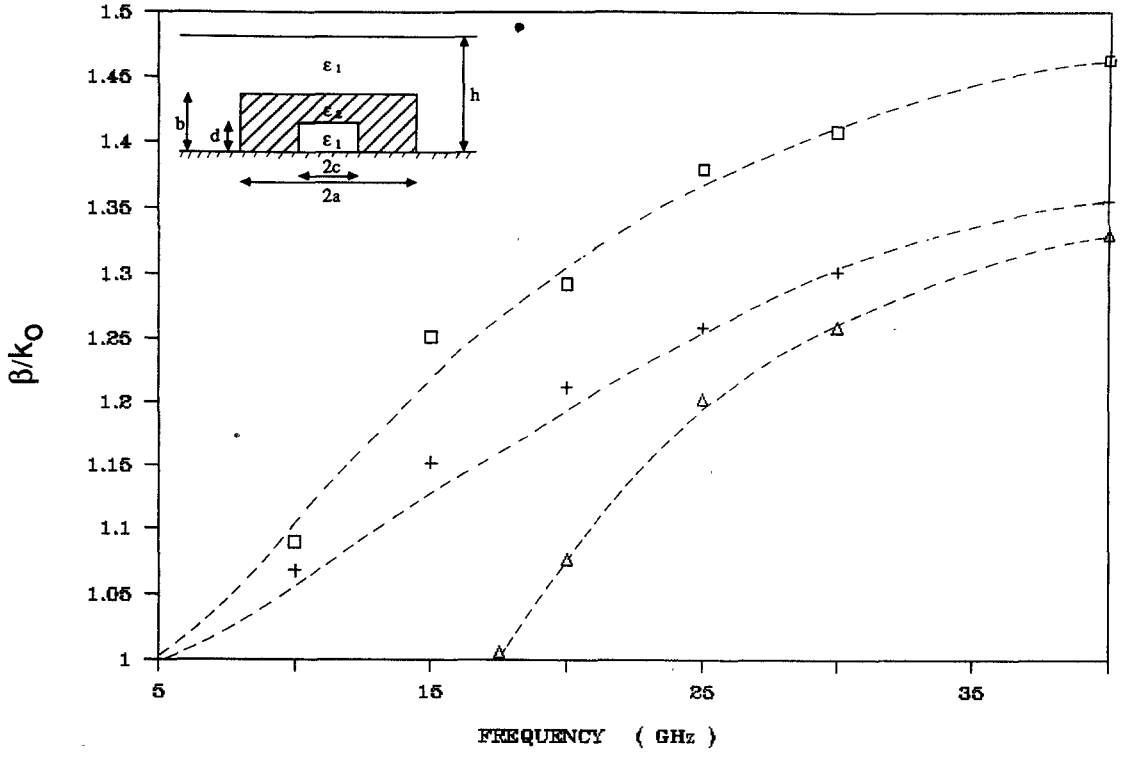

Fig. 6. Dispersion characteristics of the hollow rectangular image waveguide. □: image waveguide; +: even mode; Δ: odd mode; ----: ref. [10]; □, +, Δ: our results. $a = b = 6$ mm, (*1*) $c = 0$ mm, (*2*) $c = 3$ mm, $d = c$, $h = 1$ m, $\epsilon_{r1} = 1$, $\epsilon_{r2} = 2.23$.

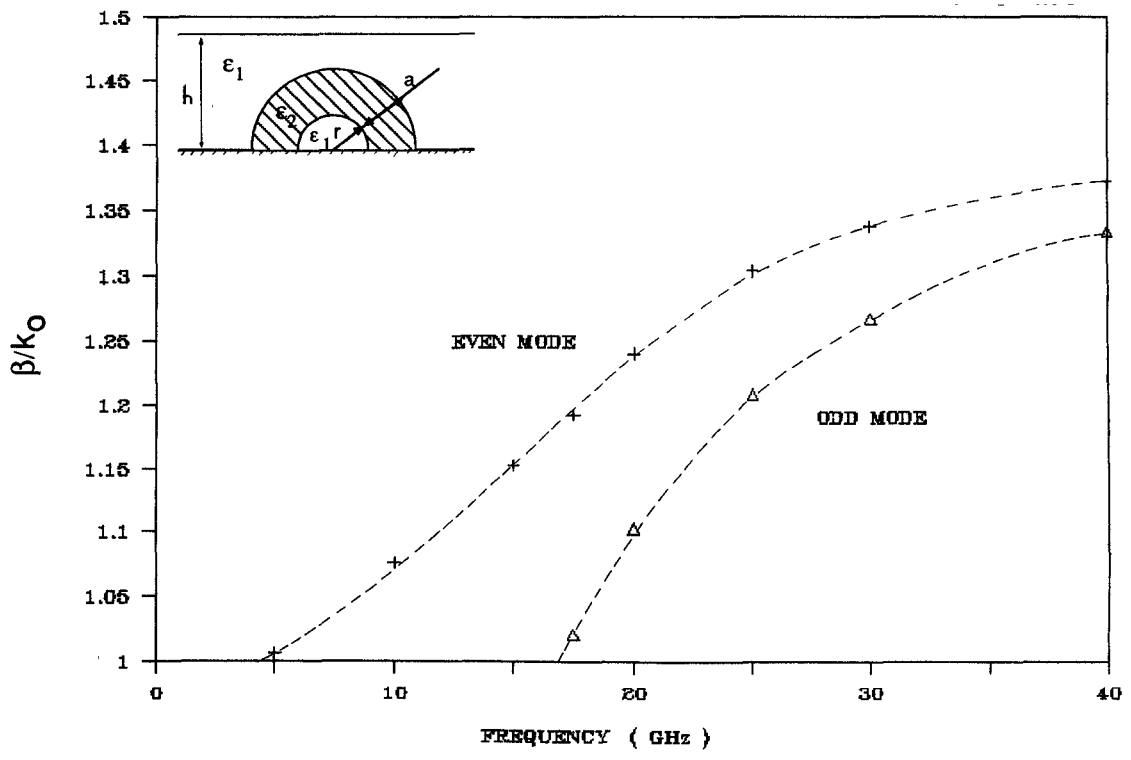

Fig. 7. Dispersion characteristics of the hollow circular image waveguide. $r = a = 3$ mm, $h = 1$ m, $\epsilon_{r1} = 1$, $\epsilon_{r2} = 2.23$.

If magnetic sidewalls are assumed for the structure, then the functions Φ_e and Φ_h can be expressed in the form

$$\Phi_e(y) = \cos \beta_n y \qquad \Phi_h(y) = \sin \beta_n y.$$

But in the case of electric sidewalls Φ_e and Φ_h will be

$$\Phi_e(y) = \sin \beta_n y \qquad \Phi_h(y) = \cos \beta_n y$$

Appendix II

By using (12), (2), and (3) yield

$$\sum_{t=1}^{N_t} \left\{ \left(1 - \hat{G}_{e12}^{tt}\right) \begin{bmatrix} E_t^t \\ E_{t+1}^t \end{bmatrix} - \sum_{j=1}^{N_t} \hat{G}_{e12}^{tj} [\phi_1 \phi_2] \begin{bmatrix} E_j^t \\ E_{j+1}^t \end{bmatrix} - \sum_{j=1}^{N_t} \left[\frac{c_2}{c_1} \hat{G}_{e11}^{tj} [\phi_1 \phi_2] \begin{bmatrix} \partial_n E_j^t \\ \partial_n E_{j+1}^t \end{bmatrix} + \frac{a}{2c_1} \hat{G}_{e11}^{tj} [-11] \begin{bmatrix} H_j^t \\ H_{j+1}^t \end{bmatrix} \right] \right\} = 0$$

$$\sum_{t=1}^{N_t} \left\{ \left(1 - \hat{G}_{h12}^{tt}\right) [\phi_1 \phi_2] \begin{bmatrix} H_t^t \\ H_{t+1}^t \end{bmatrix} - \sum_{j=1}^{N_t} \hat{G}_{h12}^{tj} [\phi_1 \phi_2] \begin{bmatrix} H_j^t \\ H_{j+1}^t \end{bmatrix} - \sum_{j=1}^{N_t} \left[\frac{b_2}{b_1} \hat{G}_{h11}^{tj} [\phi_1 \phi_2] \begin{bmatrix} \partial_n H_j^t \\ \partial_n H_{j+1}^t \end{bmatrix} + \frac{a}{2b_1} \hat{G}_{h11}^{tj} [-11] \begin{bmatrix} E_j^t \\ E_{j+1}^t \end{bmatrix} \right] \right\} = 0$$

$$\sum_{t=1}^{N_t} \left\{ \left(1 + \hat{G}_{e22}^{tt}\right) [\phi_1 \phi_2] \begin{bmatrix} E_t^t \\ E_{t+1}^t \end{bmatrix} + \sum_{j=1}^{N_t} \hat{G}_{e22}^{tj} [\phi_1 \phi_2] \begin{bmatrix} E_j^t \\ E_{j+1}^t \end{bmatrix} - \sum_{j=1}^{N_t} \hat{G}_{e21}^{tj} [\phi_1 \phi_2] \begin{bmatrix} \partial_n E_j^t \\ \partial_n E_{j+1}^t \end{bmatrix} \right\} = 0$$

$$\sum_{t=1}^{N_t} \left\{ \left(1 + \hat{G}_{h22}^{tt}\right) [\phi_1 \phi_2] \begin{bmatrix} H_t^t \\ H_{t+1}^t \end{bmatrix} + \sum_{j=1}^{N_t} \hat{G}_{h22}^{tj} [\phi_1 \phi_2] \begin{bmatrix} H_j^t \\ H_{j+1}^t \end{bmatrix} - \sum_{j=1}^{N_t} \hat{G}_{h21}^{tj} [\phi_1 \phi_2] \begin{bmatrix} \partial_n H_j^t \\ \partial_n H_{j+1}^t \end{bmatrix} \right\} = 0.$$

References

[1] W. Schlosser and H. G. Unger, "Partially filled waveguides and surfaces waveguides of rectangular cross section," in *Advances in Microwaves*, vol. 1. New York: Acadamic Press, 1966, pp. 319–387.

[2] E. A. J. Marcatili, "Dielectric rectangular waveguide and directional coupler for integrated optics," *Bell Syst. Tech. J.*, vol. 48, pp. 2071–2102, Sept. 1969.

[3] J. E. Goell, "A circular harmonic computer analysis of rectangular dielectric waveguides," *Bell Syst. Tech. J.*, vol. 48, pp. 2133–2160, Apr. 1969.

[4] E. A. J. Marcatili, "Bend in optical dielectric guides," *Bell Syst. Tech. J.*, vol. 48, pp. 2103–2132, Mar. 1969.

[5] Kazuhiko Ogusu, "Numerical analysis of the rectangular dielectric waveguide and its modifications," *IEEE Trans. Microwave Theory Tech.*, vol. MTT-25, pp. 874–880, Nov. 1977.

[6] K. Solbach and I. Wolff, "The electromagnetic fields and the phase constant of dielectric image lines," *IEEE Trans. Microwave Theory Tech.*, vol. MTT-26, pp. 266–274, Apr. 1978.

[7] S. Shindo and T. Itanami, "Low loss in rectangular dielectric image line for millimeter wave intergrated circuit," *IEEE Trans. Microwave Theory Tech.*, vol. MTT-26, pp. 747–751, Oct. 1978.

[8] T. Itanami and S. Shindo, "Channel dropping filter for millimeter wave integrated circuits," *IEEE Trans. Microwave Theory Tech.*, vol. MTT-26, pp. 759–764, Oct. 1978.

[9] U. Crombach, "Analysis of single and coupled rectangular dielectric waveguides," *IEEE Trans. Microwave Theory Tech.*, vol. MTT-29, pp. 870–874, Sept. 1981.

[10] J. F. Miao and T. Itoh, "Hollow image guide and overlayed image guide coupler," *IEEE Trans. Microwave Theory Tech.*, vol. MTT-30, pp. 1826–1831, Nov. 1982.

[11] S. Kagami and I. Fukai, "Application of boundary element method to electromagnetic field problems," *IEEE Trans. Microwave Theory Tech.*, vol. MTT-32, pp. 455–461, Apr. 1984.

[12] M. Koshiba and M. Suzuki, "Application of the boundary elements method to waveguide discontinuities," *IEEE Trans. Microwave Theory Tech.*, vol. MTT-34, pp. 301–307, Feb. 1986.

[13] C. Pichot, "Exact numerical solution for the diffused channel waveguide," *Opt. Commun.*, vol. Al, pp. 169–173, Apr. 1982.

[14] J. S. Bagby, D. N. Nyquist, and B. C. Drachman, "Integral formulation for analysis of integrated dielectric waveguides," *IEEE Trans. Microwave Theory Tech.*, vol. MTT-33, pp. 906–915, Oct. 1985.

[15] E. W. Kolk, N. H. G. Baken, and H. Blok, "Domain integral equation analysis of integrated optical and ridge waveguides in stratified media," *IEEE Trans. Microwave Theory Tech.*, vol. 38, pp. 78–84, Jan. 1990.

[16] R. Ratovondrahanta, "Analyse des guides dielectriques rectangulaires par la methode de l'opérateur transverse." Thesis 7 July 1987, INP Toulouse.

[17] C. A. Brebbia, *The Boundary Element Method for Engineers*. London: Pentech Press, 1978, pp. 46–103.

[18] C. A. Brebbia and S. Walker, *Boundary Element Techniques in Engineering*. London: Butterworth, 1980, pp. 1–119.

[19] R. E. Collin, *Field Theory of Guided Waves*. New York: McGraw-Hill, 1960, pp. 43–58.

[20] R. F. Harrington, *Field Computation by Moment Methods*. New York: Macmillan, 1968, pp. 1–61.

[21] P. Morse and H. Feshback, *Methods of Theoretical Physics*. New York: McGraw-Hill, 1953, part I, pp. 791–818.

Eigenvalues for Ridged and Other Waveguides Containing Corners of Angle $3\pi/2$ or 2π by the Finite Element Method

B. Schiff

***Abstract*—Superelements have been developed to enable the finite element method to be used for computing eigenvalues of the Laplacian over domains containing reentrant corners of angle $3\pi/2$ or 2π. The superelements embody mesh refinement and include basis functions which emulate the singular behavior of the solution at the corner. Being compatible with linear or bilinear elements, the superelements are easily incorporated into standard finite element programs. The method has been used to compute TE and TM mode eigenvalues for ridged and other waveguides, and the results agree well with those obtained using various other methods.**

I. Introduction

Ridged and other waveguides whose cross sections contain one or more reentrant corners of angle $3\pi/2$ or 2π are frequently used in microwave devices and circuits. It is therefore

Manuscript received December 15, 1988; revised December 17, 1990.

The author is with the School of Mathematical Sciences, Raymond and Beverly Sackler Faculty of Exact Sciences, Tel Aviv University, Ramat Aviv, Tel Aviv, Israel.

IEEE Log Number 9144283.

0018-9480/91/0600-1034$01.00 ©1991 IEEE